Supporting information

Se-doped-induced sulfur vacancy engineering of CuCo$_2$S$_4$ nanosheets for enhanced electrocatalytic overall water splitting

Bianli Zhang, Xingyue Qian, Hui Xu, Lin Jiang, Jiawei Xia, Haiqun Chen* and Guangyu He*

Key Laboratory of Advanced Catalytic Materials and Technology, Advanced Catalysis and Green Manufacturing Collaborative Innovation Center, Changzhou University, Changzhou, Jiangsu 213164, China

* Corresponding authors.

E-mail addresses: hegy@cczu.edu.cn (G. He), 0000-0001-5100-0324

chenhq@cczu.edu.cn (H. Chen), 0000-0001-7805-6395

1. Experimental section

1.1 Characterizations

X-ray diffraction (XRD) patterns were carried out on an X-ray diffractometer with Cu Kα radiation (λ = 1.54178 Å). Raman spectra (Japan LabRAMHR evolution) of samples were collected on a Renishaw in Via-Reflex Raman microprobe. Electron paramagnetic resonance (EPR) spectra were acquired from a Bruker EMXPLUS A30. The morphologies of samples were analyzed by scanning electron microscopy (SEM, ZEISS, Germany) and transmission electron microscopy (TEM, JEOL Ltd., JEM-2100F) operated at 200 kV. X-ray photoelectron spectroscopy (XPS) was employed to

obtain chemical valence of prepared catalysts on an XPS instrument (ESCALAB 250, Thermo, USA). The binding energy (BE) was measured by confirming the C-C peak at 284.8 eV. The BET surface area and pore size distributions were characterized by N_2 adsorption/desorption isotherms performed on Micromeritics ASAP2010C equipment in static measurement mode at -196 °C. All samples were degassed at 120 °C for 24 h before measurements. The specific surface area was studied based on the Brunauer-Emmett-Teller (BET) model. The inductively coupled plasma optical emission spectrometer (ICP-OES, 720ES, Agilent, US) was used to detect the contents of catalyst.

1.2 Electrochemical measurements

All electrochemical measurements were conducted at room temperature using CHI 760E electrochemical workstation with a standard three-electrode system. Hg/HgO and graphite rod were used as reference and counter electrodes in alkaline solution, respectively. For working electrode, 4.0 mg sample and 20 μL Nafion (5 wt%) was dissolved into 480 μL solution containing 360 μL absolute ethanol and 120 μL DI water. The obtained slurry was ultrasonicated for 1 h to acquire a uniform suspension. Then, 50 μL above dispersion was dropped onto a carbon paper (1 x 1 cm^2) and dried at room temperature. The linear sweep voltammetry (LSV) curves were collected at a scan rate of 5 mV s^{-1} in 1 M KOH electrolyte. All polarization curves were corrected with 95% iR compensation with respect to the ohmic resistance of the solution. Electrochemical impedance spectra (EIS) were assessed at open-circuit potential with the frequency

range of 10^6 to 10^{-1} Hz. Long-term chronoamperometric tests were conducted at the corresponding potential.
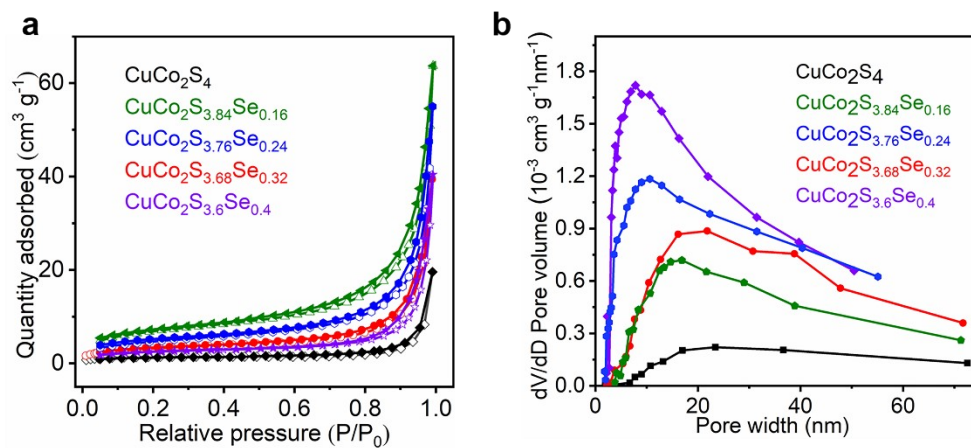

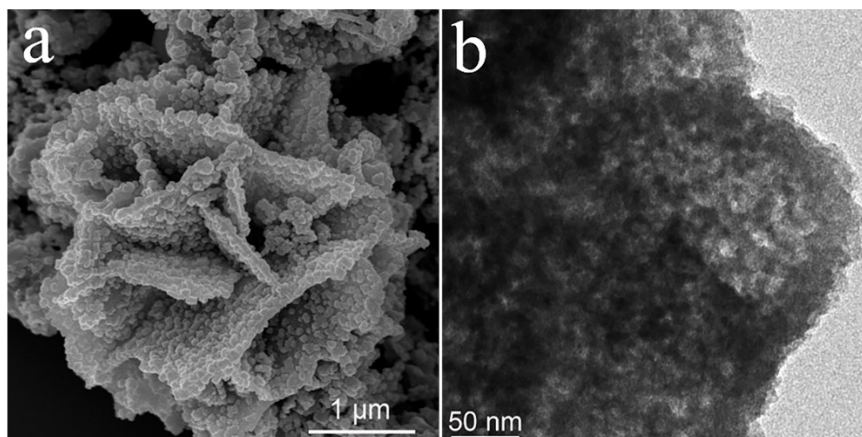**Fig. S1** N_2 adsorption/desorption isotherms of $CuCo_2S_4$ and $CuCo_2S_{4-x}Se_x$.

Fig. S2 (a) SEM and (b) TEM images of $CuCo_2S_{3.68}Se_{0.32}$ after OER test.
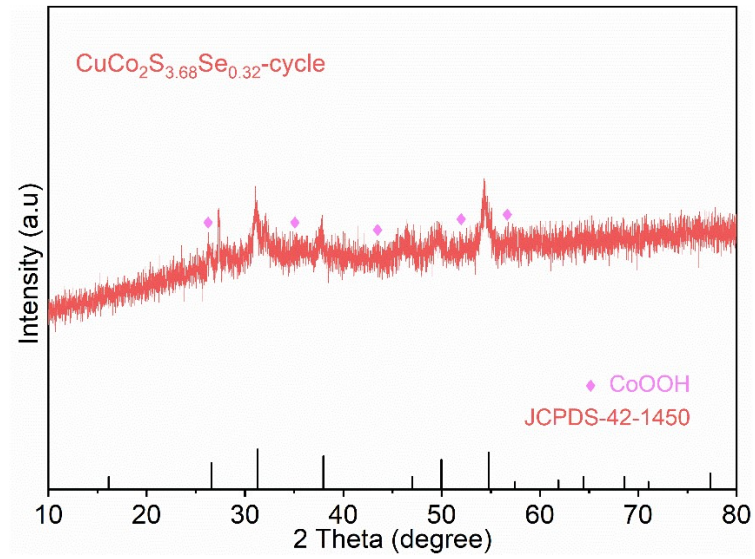
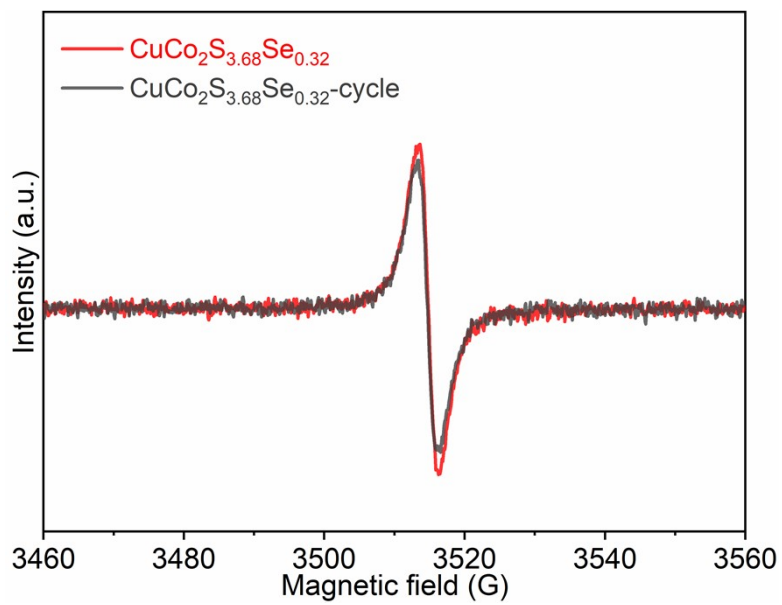**Fig. S3** XRD pattern of CuCo$_2$S$_{3.68}$Se$_{0.32}$ after a 24 h *i-t* test for OER.

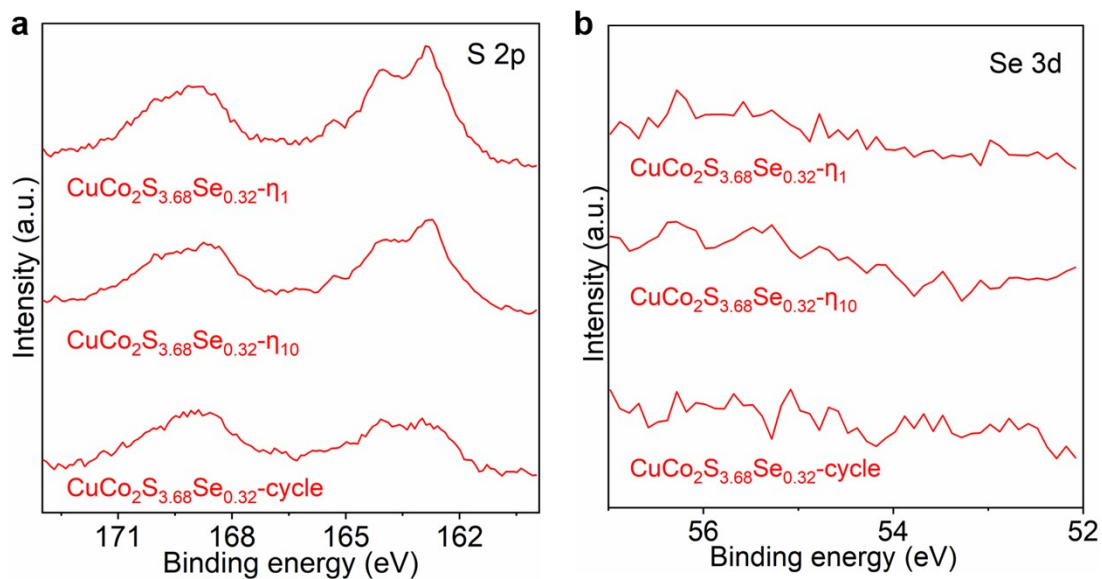**Fig. S4** EPR spectra of CuCo$_2$S$_{3.68}$Se$_{0.32}$ before and after OER test.

Fig. S5 (a) S 2p, (b)Se 3d high resolution XPS spectral of $CuCo_2S_{3.68}Se_{0.32}$ after different activation time for OER.

Fig. S6 Typical cyclic voltammetry curves of $CuCo_2S_{4-x}Se_x$ in 1M KOH for OER at the scan rates from 20 to 200 mV s^{-1}.

Fig. S7 Chronoamperometric (*i-t*) curves of the $CuCo_2S_{3.68}Se_{0.32}$ electrode at current densities of 100 mA cm^{-2} over 50 h.

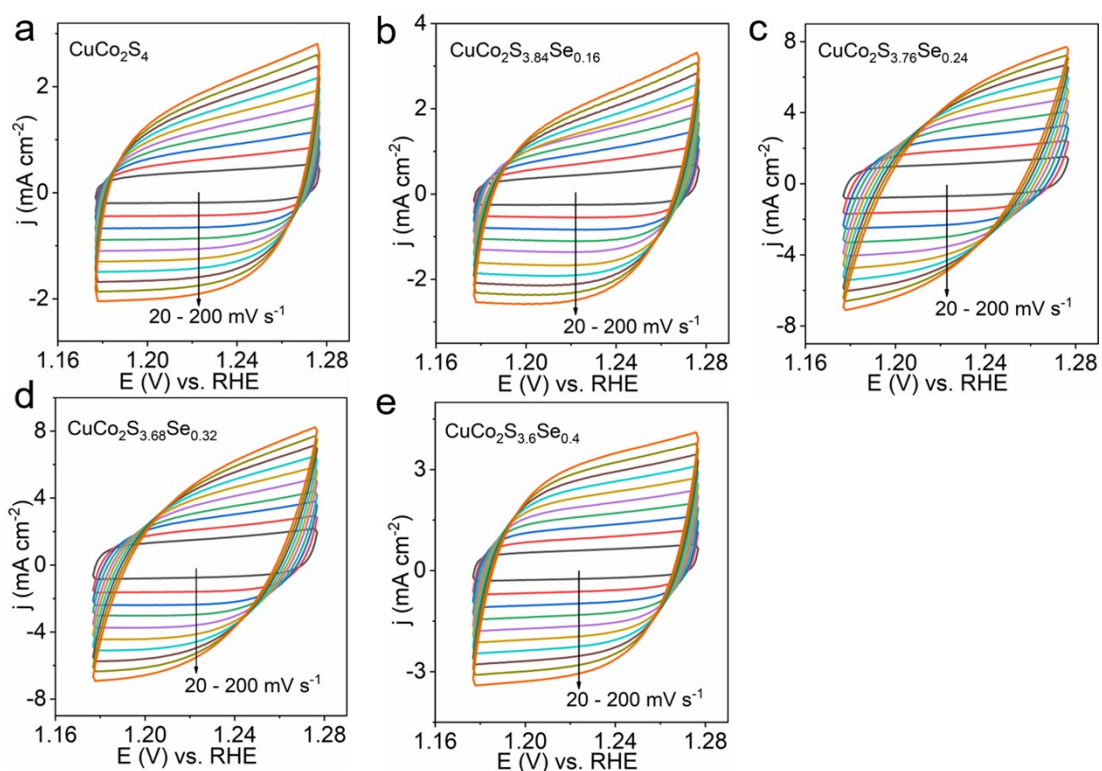**Fig. S8** Cyclic voltammetry (CV) curves of $CuCo_2S_{3.68}Se_{0.32}$ and $CuCo_2S_4$.
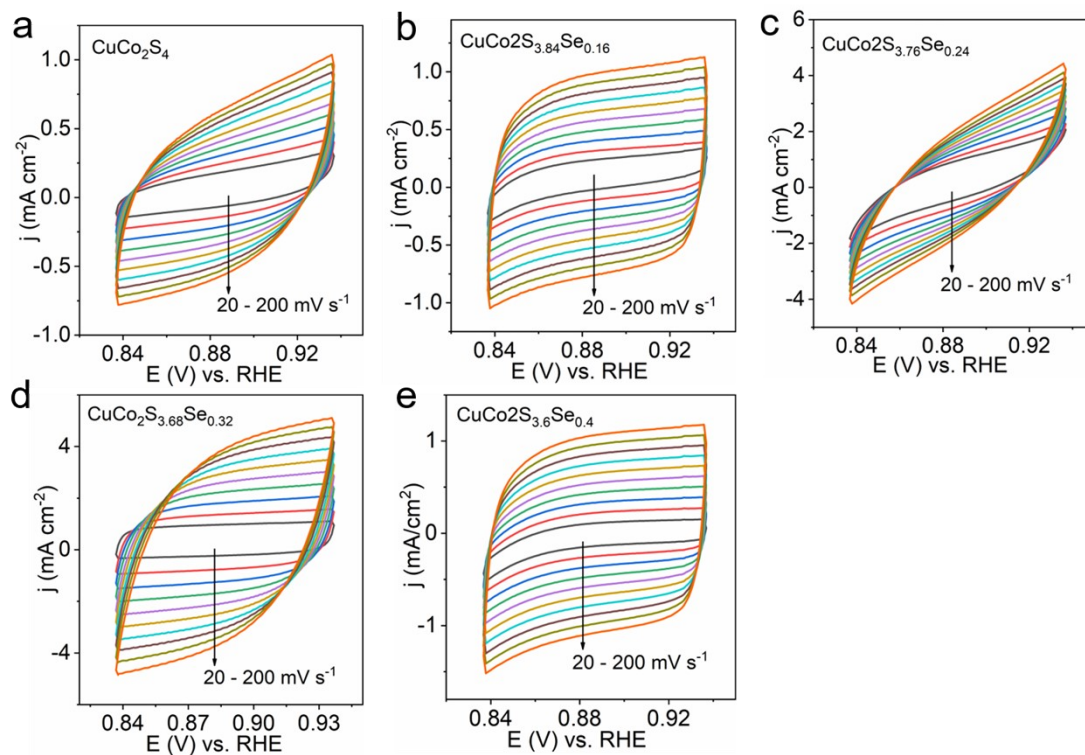
Fig. S9 Typical cyclic voltammetry curves of $CuCo_2S_{4-x}Se_x$ in 1M KOH for HER at the scan rates from 20 to 200 mV s^{-1}.
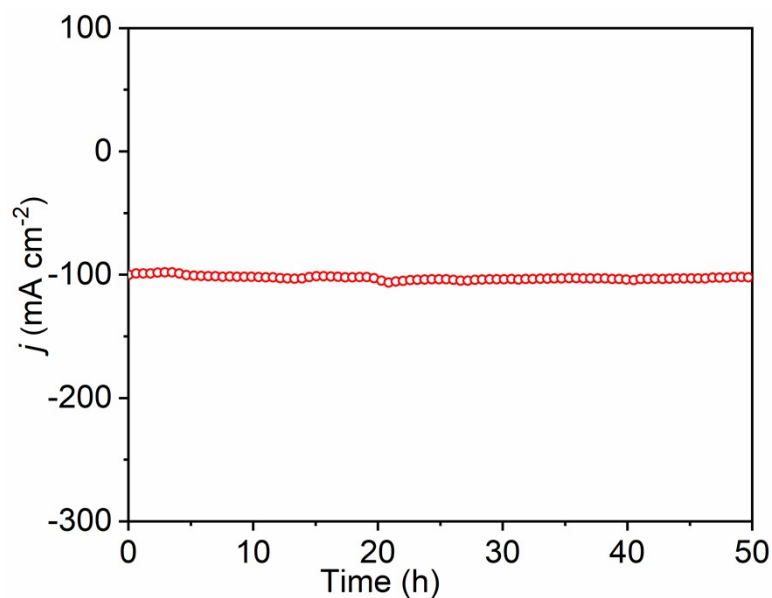
Fig. S10 Chronoamperometric (*i-t*) curves of the $CuCo_2S_{3.68}Se_{0.32}$ electrode at current densities of -100 mA cm^{-2} over 50 h.

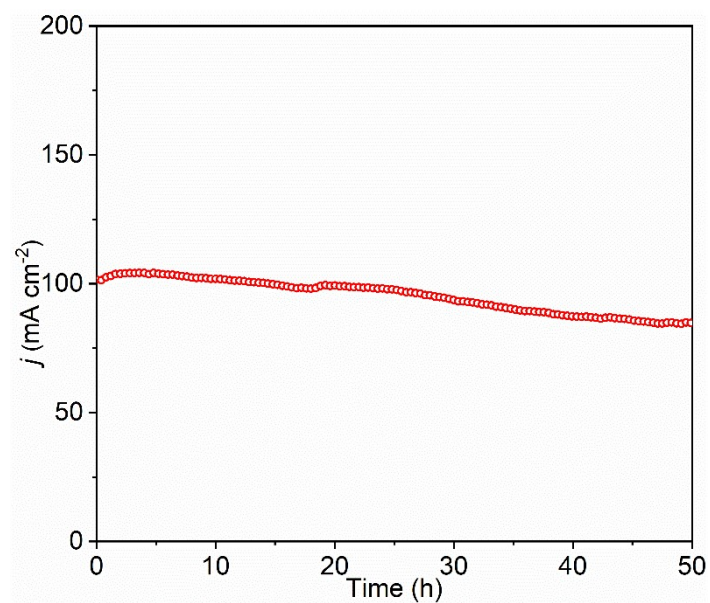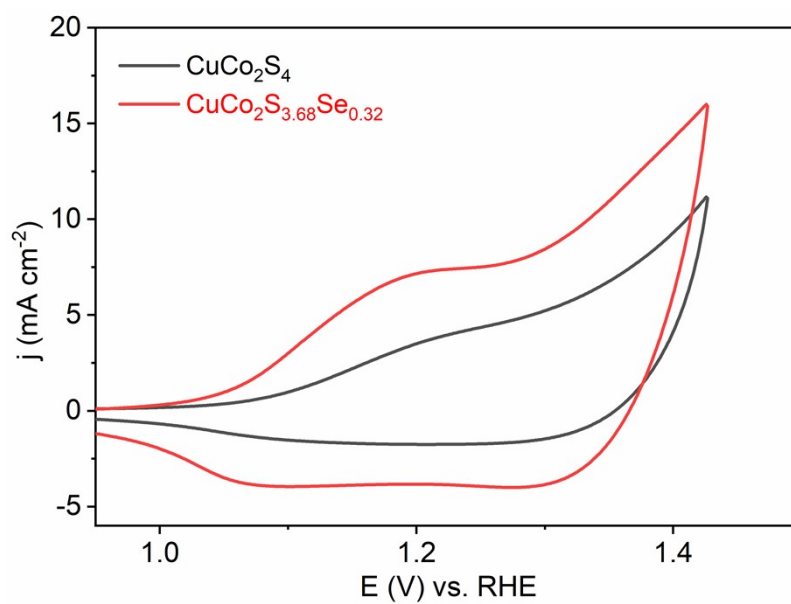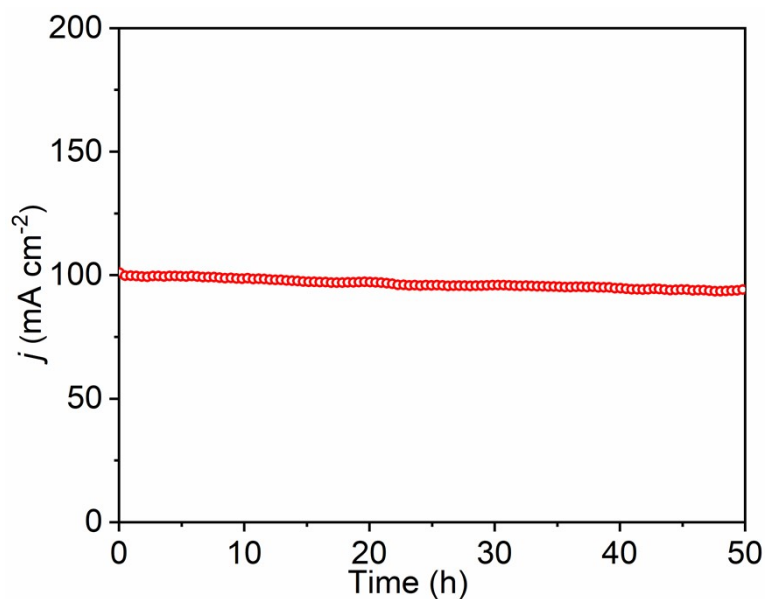**Fig. S11** Chronoamperometric (*i-t*) curves of the $CuCo_2S_{3.68}Se_{0.32}$ electrode at current densities of 100 mA cm^{-2} over 50 h for overall water-splitting.

Table S1. BET parameters of the as-prepared $CuCo_2S_4$ and $CuCo_2S_{3.68}Se_{0.32}$ samples.

Sample	BET specific surface area ($m^2\ g^{-1}$)
$CuCo_2S_4$	4.56
$CuCo_2S_{3.84}Se_{0.16}$	7.68
$CuCo_2S_{3.76}Se_{0.24}$	9.06
$CuCo_2S_{3.68}Se_{0.32}$	11.25
$CuCo_2S_{3.6}Se_{0.4}$	10.13

Table S2. The weight percentage content of elements in $CuCo_2S_{4-x}Se_x$ from ICP and elemental analysis data.

Sample	S (wt %)	Se (wt %)
$CuCo_2S_{3.84}Se_{0.16}$	32.15	3.12
$CuCo_2S_{3.76}Se_{0.24}$	30.14	4.85
$CuCo_2S_{3.68}Se_{0.32}$	29.80	6.09
$CuCo_2S_{3.6}Se_{0.4}$	28.83	7.66

Table S3. Peak area ratios and Co atomic ratios of different samples in the XPS spectra.

Sample	Co^{2+}	Co^{3+}	Co^{2+}/Co^{3+}
$CuCo_2S_4$	0.49	0.51	0.96
$CuCo_2S_{3.84}Se_{0.16}$	0.51	0.49	1.04
$CuCo_2S_{3.76}Se_{0.24}$	0.52	0.48	1.08
$CuCo_2S_{3.68}Se_{0.32}$	0.62	0.38	1.63
$CuCo_2S_{3.6}Se_{0.4}$	0.51	0.49	1.04

Table S4. Peak area ratios and Cu atomic ratios of different samples in the XPS spectra.

Sample	Cu^+	Cu^{2+}	Cu^+/Cu^{2+}
$CuCo_2S_4$	0.75	0.25	3.00
$CuCo_2S_{3.84}Se_{0.16}$	0.76	0.24	3.17
$CuCo_2S_{3.76}Se_{0.24}$	0.78	0.22	3.54
$CuCo_2S_{3.68}Se_{0.32}$	0.84	0.16	5.25
$CuCo_2S_{3.6}Se_{0.4}$	0.79	0.21	3.76

Table S5. Peak area ratios and S atomic ratios of different samples in the XPS spectra.

Sample	$S\ 2p_{1/2}$	$S\ 2p_{3/2}$	$2p_{1/2}/2p_{3/2}$
$CuCo_2S_4$	0.21	0.48	0.44
$CuCo_2S_{3.84}Se_{0.16}$	0.23	0.49	0.47
$CuCo_2S_{3.76}Se_{0.24}$	0.25	0.36	0.69
$CuCo_2S_{3.68}Se_{0.32}$	0.44	0.29	1.52
$CuCo_2S_{3.6}Se_{0.4}$	0.40	0.33	1.21

Table S6. Peak area ratios and Co atomic ratios of different activation time in the XPS spectra.

Sample	Co^{2+}	Co^{3+}	Co^{3+}/Co^{2+}
$CuCo_2S_{3.68}Se_{0.32}$	0.62	0.38	0.59
$CuCo_2S_{3.68}Se_{0.32}-\eta_1$	0.53	0.47	0.89
$CuCo_2S_{3.68}Se_{0.32}-\eta_{10}$	0.48	0.52	1.08
$CuCo_2S_{3.6}Se_{0.4}$-cycle	0.41	0.59	1.44

Table S7. Peak area ratios and Cu atomic ratios of different activation time in the XPS spectra.

Sample	Cu^{2+}	Cu^+	Cu^{2+}/Cu^+
$CuCo_2S_{3.68}Se_{0.32}$	0.16	0.84	1.63
$CuCo_2S_{3.68}Se_{0.32}-\eta_1$	0.54	0.46	0.89
$CuCo_2S_{3.68}Se_{0.32}-\eta_{10}$	0.60	0.40	1.08
$CuCo_2S_{3.6}Se_{0.4}$-cycle	0.64	0.36	1.78

Table S8. Comparison of OER performance for reported electrocatalysts.

Catalyst	Mass loading (mg cm^{-2})	OER η_{10} (mV)	Tafel slope (mV dec^{-1})	Ref.
$CuCo_2S_{3.68}Se_{0.32}$	0.4	230	58	This work
Ru-Co/ELCO	1.0	295	58.8	[1]
$LiCoO_{1.8}Cl_{0.2}$	0.4	270	55.4	[2]
$Zn_{0.2}Co_{0.8}OOH$	0.2	235	35.7	[3]
$CoSe_2-D_{Fe}-V_{Co}$	0.12	310	53.5	[4]
$NiMoO_4$	0.26	351	69	[5]
$LiCo_{0.8}Fe_{0.2}O_2$	0.23	340	50	[6]
$KxCoFe_{0.12}O_2$	1.0	290	50	[7]
$La_{0.7}Sr_{0.3}CoO_{3-\delta}$	0.35	326	70.8	[8]
Fe_2Co-GNCL	0.26	350	70	[9]
CoFe-MOF	0.21	265	44.0	[10]
CoFe 2D MOFs	0.35	274	46.7	[11]

Table S9. Comparison of HER performance for reported electrocatalysts.

Catalyst	Mass loading (mg cm^{-2})	OER η_{10} (mV)	Tafel slope (mV dec^{-1})	Ref.
$CuCo_2S_{3.68}Se_{0.32}$	0.4	65	64	This work
Co/Co_3O_4	0.85	~90	44	[12]
Co@C/NC	0.4	174.5	95.1	[13]
Co-Fe-P	0.29	86	66	[14]
CS@CNC NAs/CC	2.2	84	38	[15]
$Cu-Co-P_{20}$	0.9	138	48	[16]
NCF-MOF	0.5	270	114	[17]
Co_{50}-Mo_2C-12	0.2	125	70.95	[18]
$CN/CNL/MoS_2/CP$	0.2	106	117	[19]
CoP@N,S-3D-GN	0.2	118	50	[20]
$Ni_{0.67}Co_{0.33}/Ni_3S_2$@NF	2.0	87	80	[21]

Table S10. Comparison of overall water splitting (OWS) performance with other bifunctional electrocatalysts.

Catalyst	Mass loading (mg cm^{-2})	OWS P$_{10}$ (V)	Ref.
CuCo$_2$S$_{3.68}$Se$_{0.32}$	0.4	1.52	This work
ZnCoS-NSCNT/NP	1.0	1.59	[22]
Co$_2$P/CoP@Co@NCNT	4.3	1.60	[23]
Co-NC@Ni$_2$Fe-LDH	1.8	1.55	[24]
Co/Mo$_2$C@C	0.34	1.59	[25]
NCS/NS-rGO	0.2	1.58	[26]
CMC/750SA	0.36	1.589	[27]
10:MoCo-VS$_2$	2.0	1.54	[28]
Co-CoO/Ti$_3$C$_2$-MXene	2.0	1.55	[29]

*P$_{10}$: The required a cell voltage to drive a current density of 10 mA·cm^{-2}.

References

[1] X. Zheng, J. Yang, Z. Xu, Q. Wang, J. Wu, E. Zhang, S. Dou, W. Sun, D. Wang and Y. Li, *Angew. Chem., Int. Ed.*, 2022, **61**, e202205946.

[2] J. Wang, S. J. Kim, J. Liu, Y. Gao, S. Choi, J. Han, H. Shin, S. Jo, J. Kim, F. Ciucci, H. Kim, Q. Li, W. Yang, X. Long, S. Yang, S. P. Cho, K. H. Chae, M. G. Kim, H. Kim and J. Lim, *Nat. Catal.*, 2021, **4**, 212-222.

[3] Z.F. Huang, J. Song, Y. Du, S. Xi, S. Dou, J.M.V. Nsanzimana, C. Wang, Z.J. Xu and X. Wang, *Nat. Energy*, 2019, **4**, 329-338.

[4] Y. Dou, C. T. He, L. Zhang, H. Yin, M. Al-Mamun, J. Ma and H. Zhao, *Nat. Commun.*, 2020, **11**, 1664.

[5] C. Ye, J. Liu, Q. Zhang, X. Jin, Y. Zhao, Z. Pan, G. Chen, Y. Qiu, D. Ye, L. Gu, G. I. N. Waterhouse, L. Guo and S. Yang, *J. Am. Chem. Soc.*, 2021, **143**, 14169-14177.

[6] Y. Zhu, W. Zhou, Y. Chen, J. Yu, M. Liu and Z. Shao, *Adv. Mater.*, 2015, **27**, 7150-7155.

[7] Y. K. Sonia, M. K. Paliwal and S. K. Meher, *Sustain. Energy Fuels*, 2021, **5**, 973-985.

[8] Y. Lu, A. Ma, Y. Yu, R. Tan, C. Liu, P. Zhang, D. Liu and J. Gui, *ACS Sustainable Chem. Eng.*, 2019, **7**, 2906-2910.

[9] Y. S. Wei, L. Sun, M. Wang, J. Hong, L. Zou, H. Liu, Y. Wang, M. Zhang, Z. Liu, Y. Li, S. Horike, K. Suenaga and Q. Xu, *Angew. Chem., Int. Ed.*, 2020, **59**, 16013-16022.

[10] Z. Zou, T. Wang, X. Zhao, W.-J. Jiang, H. Pan, D. Gao and C. Xu, *ACS Catal.* 2019, **9**, 7356-7364.

[11] M. Cai, Q. Liu, Z. Xue, Y. Li, Y. Fan, A. Huang, M. R. Li, M. Croft, T. A. Tyson, Z. Ke and G. Li, *J. Mater. Chem. A*, 2020, **8**, 190-195.

[12] X. Yan, L. Tian, M. He and X. Chen, *Nano Lett.*, 2015, **15**, 6015-6021.

[13] Q. Wang, K. Cui, D. Liu, Y. Wu and S. Ren, *Energy Fuels*, 2022, **36**, 1688-1696.

[14] J. Chen, J. Liu, J. Q. Xie, H. Ye, X. Z. Fu, R. Sun and C. P. Wong, *Nano Energy*, 2019, **56**, 225-233.

[15] F. Tian, S. Geng, L. He, Y. Huang, A. Fauzi, W. Yang, Y. Liu and Y. Yu, *Chem. Eng. J.*, 2021, **417**, 129232.

[16] Y Y. S. Park, W. S. Choi, M. J. Jang, J. H. Lee, S. Park, H. Jin, M. H. Seo, K. H. Lee, Y. Yin, Y. Kim, J. Yang and S. M. Choi, *ACS Sustainable Chem. Eng.*, 2019, **7**, 10734-10741.

[17] W. Ahn, M. G. Park, D. U. Lee, M. H. Seo, G. Jiang, Z. P. Cano, F. M. Hassan and Z. Chen, *Adv. Funct. Mater.*, 2018, **28**, 1802129.

[18] Y. Ma, M. Chen, H. Geng, H. Dong, P. Wu, X. Li, G. Guan and T. Wang, *Adv. Funct. Mater.*, 2020, **30**, 2000561.

[19] J. Dong, X. Zhang, J. Huang, J. Hu, Z. Chen and Y. Lai, *Chem. Eng. J.*, 2021, **412**, 128556.

[20] C. Karaman, O. Karaman, N. Atar and M. L. Yola, *Electrochimica Acta*, 2021, **380**, 138262.

[21] Z. Wu, Y. Feng, Z. Qin, X. Han, X. Zheng, Y. Deng and W. Hu, *Small*, 2022, **18**, 2106904.

[22] Z. Yu, Y. Bai, S. Zhang, Y. Liu, N. Zhang and K. Sun, *J. Mater. Chem. A*, 2018, **6**, 10441-10446.

[23] D. Fa, Y. Tao, X. Pan, D. Wang, G. Feng, J. Yuan, Q. Luo, Y. Song, X. J. Gao, L. Yang, S. Lei and W. Hu, *Angew Chem. Int. Ed.* , 2022, **61**, e202207845.

[24] T. Guo, L. Chen, Y. Li and K. Shen, *Small*, 2022, **18**, 2107739.

[25] S. Yuan, M. Xia, Z. Liu, K. Wang, L. Xiang, G. Huang, J. Zhang and N. Li, *Chem. Eng. J.*, 2022, **430**, 132697.

[26] H. Li, L. Chen, P. Jin, Y. Li, J. Pang, J. Hou, S. Peng, G. Wang and Y. Shi, *Nano Res.*, 2022, **15**, 950-958.

[27] W. Yaseen, M. Xie, B. A. Yusuf, Y. Xu, N. Ullah, M. Rafiq, A. Ali and J. Xie, *Appl. Surf. Sci.*, 2022, **579**, 152148.

[27] V. K. Singh, U. T. Nakate, P. Bhuyan, J. Chen, D. T. Tran and S. Park, *J. Mater. Chem. A*, 2022, **10**, 9067-9079.

[29] D. Guo, X. Li, Y. Jiao, H. Yan, A. Wu, G. Yang, Y. Wang, C. Tian and H. Fu, *Nano Res.*, 2022, **15**, 238-247.